STAU2 Protein Level is Controlled by Caspases and the CHK1 Pathway and Regulates Cell Cycle Progression in the Non-transformed hTERT-RPE1 Cells

Lionel Conde
Universite de Montreal
Remy Beaujois
Universite de Montreal
Luc DesGroseillers (luc.desgroseillers@umontreal.ca)
Département de biochimie et médecine moléculaire, Faculté de médecine, Université de Montréal, 2900 Édouard Montpetit Montréal, QC, Canada. https://orcid.org/0000-0002-1511-8998

Research article

Keywords: Staufen2, CHK1, caspase, cell proliferation

DOI: https://doi.org/10.21203/rs.3.rs-60003/v1

Abstract

Background: Staufen2 (STAU2) is an RNA binding protein involved in the posttranscriptional regulation of gene expression. In neurons, STAU2 is required to maintain the balance between differentiation and proliferation of neural stem cells through asymmetric cell division. However, the importance of controlling STAU2 expression for cell cycle progression is not clear in non-neuronal dividing cells. We recently showed that STAU2 transcription is inhibited in response to DNA-damage due to E2F1 displacement from the *STAU2* gene promoter. We now study the regulation of STAU2 steady-state levels in unstressed cells and its consequence for cell proliferation.

Results: CRISPR/Cas9-mediated and RNAi-dependent STAU2 depletion in the non-transformed hTERT-RPE1 cells both facilitate cell proliferation suggesting that STAU2 expression influences pathway(s) linked to cell cycle controls. Such effects are not observed in the CRISPR STAU2-KO cancer HCT116 cells nor in the STAU2-RNAi-depleted HeLa cells. Interestingly, a physiological decrease in the steady-state level of STAU2 is controlled by caspases. This effect of peptidases is counterbalanced by the activity of the CHK1 pathway suggesting that STAU2 partial degradation/stabilization fines tune cell cycle progression in unstressed cells. A large-scale proteomic analysis using STAU2/biotinylase fusion protein identifies known STAU2 interactors involved in RNA translation, localization, splicing, or decay confirming the role of STAU2 in the posttranscriptional regulation of gene expression. In addition, several proteins found in the nucleolus, including proteins of the ribosome biogenesis pathway and of the DNA damage response, are found in close proximity to STAU2. Strikingly, many of these proteins are linked to the kinase CHK1 pathway, reinforcing the link between STAU2 functions and the CHK1 pathway. Indeed, inhibition of the CHK1 pathway dissociates STAU1 from proteins involved in translation and RNA metabolism.

Conclusions: These results indicate that STAU2 is involved in pathway(s) that control(s) cell proliferation, likely via mechanisms of posttranscriptional regulation, ribonucleoprotein complex assembly, genome integrity and/or checkpoint controls. This novel function of STAU2 is regulated by caspases and by the kinase CHK1 pathway.

Background

RNA-binding proteins (RBPs) and the posttranscriptional regulation of gene expression that they impose on their associated RNAs play crucial role in cells [1–3]. They group mRNAs within regulons coding for functionally-related proteins and allow a timely control of protein synthesis in response to changing cellular environments [4]. RBPs are involved in diverse biological processes that include cell proliferation, DNA damage response and metabolism [5]. Given the broad spectrum of biological functions that depend on RBP activity, it is not surprising that many studies showed that their overexpression or depletion result in strong cellular phenotypes, indicating that their expression levels have to be tightly controlled. Moreover, mutations in genes that code for RBPs are linked to numerous diseases including neurological disorders and various types of cancer [6, 7].

Staufen2 (STAU2) is an RNA-binding protein [8, 9] that binds mRNAs coding for proteins involved in multiple cellular processes including cell cycle regulation [10]. The *STAU2* gene, through differential splicing, generates several isoforms, the major ones having molecular masses of 52, 59 and 62 kDa [9]. STAU2 isoforms are mostly cytoplasmic, localizing near the endoplasmic reticulum [9], but can also be found in the nucleus and nucleolus [11]. STAU2 regulates mRNA expression through several posttranscriptional molecular processes such as mRNA localization, differential splicing, regulation of translation, and mRNA decay [12–16]. The physiological consequences of STAU2 downregulation was studied in several animal models. In zebrafish, Stau2 is required for the migration of primordial germ cells and for survival of neurons in the central nervous system [17]. In Xenopus, Stau2 controls the anterior endodermal organ formation [18]. In mouse oocytes, STAU2 is needed for meiosis progression and spindle integrity [19]. In chicken, STAU2 downregulation induces small eye development as a consequence of reduced cell proliferation [20]. Likewise, in developing mouse cortex, STAU2 regulates the balance between neural stem cell maintenance and differentiation [21, 22]: STAU2 downregulation induces cell differentiation while its overexpression produces periventricular neuronal masses. STAU2 depletion in mouse and rat brains inpairs hippocampal spatial working memory, spatial novelty detection and/or associative learning and memory [23, 24]. This is consistent with the importance of STAU2 for dendritic spine morphogenesis and for long-term synaptic depression [13, 15]. STAU2 is also linked to the DNA damage response and the apoptotic pathway since STAU2 depletion causes an accumulation of DNA damage and facilitates apoptosis in the HCT116 cancer cell line [25]. In addition, induction of single-stranded break causes the inhibition of STAU2 transcription as a consequence of delocalization of the transcription factor E2F1 from the *STAU2* promoter [25].

In this paper, we now show that STAU2 knockout facilitates cell proliferation in the non-transformed hTERT-RPE1 cells. We further show that STAU2 protein steady-state level is stabilized by the CHK1 pathway and is decreased by the activity of caspases in unstressed cells. Finally, a genome wide approach reveals that STAU2 is in close proximity to proteins involved in the posttranscriptional regulation of gene expression and to proteins of the nucleolus, including proteins linked to ribosome biogenesis and to DNA repair. Altogether, our results identify novel STAU2 functions at the crossroad of cell cycle regulation and DNA damage response.

Results

STAU2 depletion facilitates proliferation of non-transformed hTER-RPE1 cells

To study the role of STAU2 in unstressed cells, we first generated STAU2 knockout (STAU2-KO) cells using the non-transformed hTERT-RPE1 cells and the CRISPR/Cas9 technology (Additional Fig S1). Cells were transfected with a plasmid expressing CRISPR/Cas9 and an RNA guide targeting exon 6 of the *STAU2* gene. This exon is just downstream of the AUG initiation codon and common to all STAU2 isoforms. Individual clones were isolated and tested for STAU2 expression by dot blotting (Additional Fig S1B)

revealing that 26% of the selected clones were negative for STAU2 expression. DNA sequencing of *STAU2* exon 6 of two STAU2-KO clones showed the presence of short deletions that introduced premature stop codons (Additional Fig S1A). RT-qPCR quantification revealed that STAU2 mRNA levels were also decreased in all tested clones compared to that in wild type (WT) cells (Additional Fig S1C).

To determine the impact of STAU2 knockout on cell proliferation, we studied the growth of several STAU2-KO clones compared to that of WT hTERT-RPE1 cells (Fig. 1A). Using the growth curve assay, we first showed that the STAU2-KO clone A4 proliferated faster than wild type cells, indicating that STAU2 depletion interferes with cell cycle progression and potentiates cell growth (Fig. 1A). To rule out a putative off-target effect, we used the colony growth assay to monitor proliferation of additional STAU2-KO clones. Proliferation was significantly increased in the three tested clones (Fig. 1A) compared to WT hTERT-RPE1 cells. A similar increase in cell proliferation was observed in shRNA-mediated STAU2 depleted cells (Fig. 1B; Additional Fig S2). Interestingly, STAU2 depletion in HeLa tumor cells and STAU2-KO in the HCT116 cancer cell line (Additional Fig S3) had no effect on cell proliferation (Fig. 1C,D. Additional Fig S2) indicating that cancer cells can bypass the consequences of STAU2 depletion that are observed in non-transformed cells.

Caspases are involved in STAU2 degradation

These results suggest that physiological modulation of the steady-state levels of STAU2 may be advantageous for the fine tuning of cell proliferation in changing cell environment. Therefore, to identify endogenous pathway(s) that control(s) the physiological stability/degradation of STAU2, we first tested pharmacological inhibitors known to target the major protein degradation pathways. HCT116 cells were incubated with the proteasome inhibitor MG132 (Fig. 2A) for six hours or the lysosome inhibitor iLYS (Fig. 2B) for ten hours. Western blotting experiments showed that neither the proteasome inhibitor nor the lysosome inhibitor changed the steady-state levels of STAU2.

Western blot analysis of protein bands using anti-STAU2 antibody often revealed the presence of specific bands of lower molecular masses (Fig. 2A) that disappeared in STAU2-KO cells (not shown), suggesting a partial cleavage of STAU2 by specific peptidases in unstressed cells. Therefore, as STAU2 functions are linked to cell proliferation and apoptosis [25], we asked whether caspases, whose activities are, among others, linked to these processes [26], can modulate the steady-state levels of STAU2 in hTERT-RPE1 and HCT116 cells. Interestingly, the pan-caspase inhibitor ZVAD-FMK increased the steady-state levels of STAU2 indicating that caspases contribute to STAU2 degradation in unstressed cells (Fig. 2C). Concomitant with the stabilization of the full-length STAU2 protein, several bands of lower molecular weight recognized with anti-STAU2 antibody in untreated cells totally disappeared upon caspases inhibition. Incubation of HCT116 cells with another caspase inhibitor (emricasan) also protected STAU2 from degradation and prevented the generation of the shorter fragments (Fig. 2C), ruling out a putative off-target effect of the drugs. Inhibition of caspases was confirmed by the stabilization of PARP1, a known target of caspase 3. As the anti-STAU2 antibody recognized degradation products containing the N-terminal end of STAU2, we also expressed STAU2^{59}-FLAG$_3$ and used the anti-FLAG antibody in an

attempt to detect C-terminal fragments. In the presence of pan-caspase inhibitor, a specific degradation product of around 15 kDa disappeared (Fig. 2D). These results identify at least one putative caspase-cleavage site in the C-terminal end of STAU2, consistent with the prediction of three caspase sites in this area (Fig. 2D). Altogether, these results indicate that STAU2 is a substrate of caspases in unstressed cells.

STAU2 is in close proximity to proteins involved in RNA post-transcriptional regulation

As a means to identify the pathway(s) that benefits from STAU2 stabilization/degradation, we used BioID2, a genome wide approach that identifies proteins in close proximity to STAU2 (within a range of 10 nm). hTERT-RPE1 cells were infected with a virus expressing the STAU2^{52}-biotinylase-HA fusion protein. We first showed that the fusion protein localized with the same subcellular distribution as STAU2^{52}-Myc$_3$ by fluorescence microscopy (Fig. 3A) and that, in the presence of biotin, the fusion protein can covalently add biotin on proteins (Fig. 3B). Then, we incubated cells with biotin for 16 h. Cells were collected, and biotinylated proteins were pulled down with streptavidin-coupled magnetic beads. Labeled proteins were identified by mass spectrometry (Additional Table S1). Interaction probability was analyzed with SAINT (Significance Analysis of INTeractome) [27] and potentials off-targets were rejected using CRAPOME (Contaminant Repository for Affinity Purification) [28]. We identified 325 peptides using a score of 0.7 or better (Additional Table S2). Known STAU2 interactors were found in the list of biotinylated proteins, including UPF1 [16], STAU1 [29], CDK1 [30], RSL1D1 [31], ZFR [32], and PABPC1 [33], confirming the efficacy and specificity of the assay. Proteins showing the highest enrichment (fold-changes) are presented along with a heat map representing their average spectral counts (Fig. 3C). In addition, the enriched GO terms are related to known STAU2 functions, such as translation, RNA metabolism, RNA localization, ribonucleoprotein complex biogenesis, RNA decay, splicing and stress granule formation (Additional Table S3). These results indicate that the posttranscriptional regulation mediated by STAU2 can be dramatically affects upon degradation/stabilization of STAU2. Interestingly, in addition to proteins of the posttranscriptional pathways, this approach also identified numerous proteins localized in the nucleolus including proteins involved in ribosome biogenesis, response to DNA damage, DNA replication, and cell cycle regulation (Fig. 3D). STAU2-biotinylase often labeled all the proteins found within specific complexes indicating that STAU2 is in close proximity to functional complexes and not only to single proteins. For examples, not only the screen identified PRKDC (DNA-PK) but also its cofactors XRCC5 (KU80) and XRCC6 (KU70) that are recruited together at DNA damage foci [34] and all the components of the HEMIN1-DNA-PK-paraspeckel ribonucleoprotein complex [35]. Strikingly, a large percentage of the labeled proteins are linked to the CHK1 pathway, suggesting that STAU2 expression could also be modulated by this pathway.

STAU2 protein level is regulated by the CHK1 pathway

To determine if STAU2 is a downstream factor in the CHK1 pathway as suggested by the BioID2 assay, we treated the non-transformed hTERT-RPE1 and the cancer HCT116 cells with the CHK1 inhibitor PF47 for eight hours (Fig. 4A). Our results indicated that STAU2 steady-state level significantly decreased

following CHK1 inhibition. Inhibition of CHK1 by two additional inhibitors (iCHK1 and CHIR124) also resulted in STAU2 depletion (Fig. 4A), ruling out an off-target effect. Interestingly, the decrease of STAU2 protein levels happened without significant cleavage of PARP1, indicating that this effect is not an indirect consequence of apoptosis. To further eliminate putative off-target effect, we also treated cells with lower inhibitor concentrations (1 μM vs 20 μM) using longer incubation times. hTERT-RPE1 and HCT116 cells were incubated in the presence of CHK1 inhibitor PF47 for forty-eight hours, and STAU2 protein levels were quantified by Western blotting (Fig. 4B). As observed above, inhibition of CHK1 with lower inhibitor concentrations still caused a decrease in STAU2 protein levels. To study the mechanism of downregulation, STAU2 protein and mRNA levels were quantified by Western blotting and RT-qPCR (Fig. 4C), respectively. Our results indicated that STAU2 steady-state level significantly decreased following CHK1 inhibition while mRNA levels were stable. Therefore, the decrease in STAU2 protein levels did not rely on transcriptional downregulation. These results indicate that STAU2 steady-state protein level is regulated by the CHK1 pathway, likely through an active mechanism of protein degradation.

Inhibition of the CHK1 pathway dissociates STAU1 from RNA metabolism

To determine the immediate consequence of CHK1 inhibition on STAU2 proximal interactome, we identified proteins in proximity to STAU2 during the first four hours following inhibition of CHK1 by PF47 using the Turbo-biotinylase. A virus expressing STAU2^{52}/turbo-biotinylase was infected in hTERT-RPE1 cells and the activity of the fusion protein was induced by addition of biotin in the presence or absence of the CHK1 inhibitor PF47. Biotinylated proteins were isolated four hours later and analyzed by mass spectrometry (Additional Table S4). In the absence of PF47, STAU2 is in close proximity to proteins involved in translation and RNA metabolism as described above (Additional Table S5, S6). However, in the presence of PF47, 57 of the previously identified proximity partners were absent or less abundant. Proteins showing the highest fold change are presented in Fig. 4D. Proteins enriched in GO terms related to translation, miRNA metabolic processes and mRNA catabolism were lost (Additional Table S7, S8). Interestingly, this change in STAU2 interactome occurs prior to STAU2 degradation, indicating that STAU2 functions are rapidly affected in response to CHK1 inhibition, before its degradation. Interestingly, only two proteins (SMEG1 and SMEG2) increased their proximity to STAU2 in these conditions. The role of these proteins is poorly understood. They were nevertheless previously described as modulators of zinc-dependent proteases via their high capacity to binding zinc [36] and shown to co-immunoprecipitate with several proteins including proteins involved in checkpoint controls and DNA damage repair [37].

Discussion

In this paper, we investigated the consequence of STAU2 depletion in non-transformed and cancer cells. We show that STAU2 depletion accelerates cell cycle progression in non-transformed cells but not in cancer cells. Interestingly, under physiological conditions, the steady state level of STAU2 protein is controlled by caspases and by the activity of the CHK1 pathway. This loop likely contributes to the fine-

tuning of cell proliferation in changing cell environment. The regulation of STAU2 at the protein level is in addition to that already observed at the transcriptional level by the transcription factor E2F1 [25]. Regulation of STAU2 by the E2F1 and CHK1 pathways that induce and facilitate S phase progression and DNA surveillance suggests a role for STAU2 in pathways that merge with mechanisms of DNA replication and/or DNA maintenance during S phase.

STAU2 regulates cell proliferation

STAU2, as an RNA-binding protein involved in the posttranscriptional regulation of gene expression, was previously shown to bind mRNAs coding for proteins involved in cell cycle regulation and cell cycle proliferation [10], some of them having proto-oncogene or tumor suppressor functions. Notably, STAU2 was shown to bind 26 mRNAs involved in the TGF-β pathway, including the central protein TGF-β receptor I [10]. It was recently reported that dysregulation of the TGF-β pathway in RPE1 cells leads to cell cycle dysregulation and tumoral transformation [38]. The phenotypes observed upon STAU2 depletion are indeed compatible with oncogenic transformation. Oncogenic transformation was previously observed when RNA-binding proteins inappropriately misregulated proto-oncogenes and/or tumor suppressor genes [6, 39, 7, 40, 3]. The hyper-proliferative phenotype that results from the misregulation of these RNA-binding proteins is often followed by an accumulation of DNA damage due to the loss of cell cycle checkpoints [41, 42]. Accumulation of DNA damages are indeed observed in STAU2-KO hTERT-RPE1 cells (Additional Fig S4) and in RNAi-mediated STAU2 knockdown in HCT116 cells [25]. Oncogenic transformation may also explain why tumor cells are not affected by STAU2 depletion. Transformed cell lines are known to be permanently stimulated by oncogenic stimulus [43, 44], and therefore additional oncogenic stimulus may not affect their proliferation.

STAU2 protein is degraded by caspases and stabilized by the CHK1 pathway

Under physiological conditions, STAU2 protein level is decreased by caspase activity and stabilized by the CHK1 pathway. As CHK1 activation inhibits caspase activity [45], it is tempting to propose that CHK1 indirectly controls STAU2 steady-state levels via the activation/inhibition of caspase activity. Although well characterized for their roles in response to massive DNA damages and induction of apoptosis [46–50], caspases also play other important roles in unstressed cells related to cell proliferation, differentiation and cellular reprogramming [51–53]. In turn, CHK1 is involved in cell cycle control, especially during the S phase, where it is required for firing origin of DNA replication [54]. CHK1 regulates checkpoint controls and is essential for cell survival in dividing cells [55] and its inhibition induces an accumulation of DNA damage and apoptosis [56, 57].

Alternatively, CHK1 may control STAU2 stability via activation of downstream kinases as previously described for the CHK1-mediated control of the RNA-binding protein HuR via the regulation of CDK1 [58]. Interestingly, STAU2 is a target of CDK1 [30] and CDK1 was found in the list of proteins in proximity to STAU2 (Additional Table S1). In contrast, we have no evidence that STAU2 is a direct target of CHK1.

CHK1 was not found in the list of proteins in proximity to STAU2 and, using an in-vitro kinase assay, we did not observe phosphorylation of STAU2 by a purified CHK1 kinase (data not shown).

STAU2 is in close proximity to proteins involved in RNA posttranscriptional regulation and proteins of the nucleolus

Degradation/stabilization of STAU2 and/or modulation of STAU2 functions via proximal partners should influence the pathway(s) in which STAU2 is involved. The BioID2 and TurboID experiments that detect proteins in close proximity to STAU2 link STAU2 to its well recognized functions in RNA posttranscriptional regulation. Indeed, STAU2 is well known for its roles in translation [15], RNA localization [12, 9, 15], splicing [14], mRNA decay [16], and stress granule formation [59]. It is likely that STAU2 regulation by caspases and/or the CHK1 pathway fine tunes the expression of mRNA regulons, resulting in well-ordered cell proliferation.

Interestingly, these genome-wide experiments also identify many proteins that can be found in the nucleolus. The nucleolus is well known for its role in ribosome biogenesis and for its involvement in non-ribosomal ribonucleoprotein complex formation [60]. Labeling of proteins found in the nucleolus compartment is consistent with earlier observation showing that STAU2 can migrate in the nucleolus [11]. The role of STAU2 in the nucleolus is unclear but it was proposed that STAU2 may assemble ribonucleoprotein complexes in the nucleolus [61]. The presence of ribosomes in STAU2-containing ribonucleoprotein complexes [9] further suggests a functional link between ribosome biogenesis and RNP formation in the nucleolus. STAU2 indeed co-immunoprecipitates with the ribosome biogenesis factor RSL1D1 [31]. The nucleolus might function as a checkpoint to verify the potential functional integrity of RNP and RNP-ribosome complexes or to tightly regulate their activity and/or release. Depletion of STAU2 may thus cause the formation of less-functional ribonucleoprotein complexes that could be released ahead of time or in inappropriate cellular compartments, impairing cell proliferation.

Other proteins in proximity to STAU2 are members of the DNA damage response. Most of these proteins can be found in the nucleoplasm and in the nucleolus and, therefore, could be non-specifically labeled via their co-localization with STAU2 in the nucleolus. However, STAU2 depletion causes an accumulation of DNA damages and therefore could be somehow involved in processes of DNA repair. Several processes could link STAU2 to DNA repair pathways. First, rDNA genes are the most transcribed genes and thus collisions between the transcription machinery and the replication fork are frequent [62, 63]. Consistently, several proteins involved in DNA replication are found in proximity to STAU2. The clashes between the machineries lead to replication fork stalling and single-stranded breaks [60]. This, in turn, activates the CHK1 kinase pathway [64–66]. In addition, R-Loops forms between nascent mRNAs and template DNA strands leading to genomic instability [67–69]. Remarkably, dysregulation of post-transcriptional processes increases R-loops formation [67, 70]. Depletion of STAU2 may thus facilitate the formation of R-loops whereas STAU2 stabilization upon CHK1 activation may help to attenuate the effects of R-loop formation. Alternatively, several studies have revealed the importance of lncRNAs in the DNA damage repair processes [71]. lncRNAs act as scaffolds for DNA repair protein recruitment. For example, lncRNA

LINP1 participates in DNA-PK recruitment to DSB [72] and lncRNA NEAT1 is needed for the formation of DNA-PK/HEXIM1 paraspeckle complexes [35]. In other cases, lncRNAs play a role in chromatin modification, which is an indispensable step for the DNA repair process [73]. It is conceivable that STAU2 may be required to localize lncRNAs at the DNA damage sites to support the repair process.

Conlusions

In this paper, we describe a complex network of proteins in proximity to STAU2 that influences the roles of STAU2 in mRNA translation and RNA metabolism. This study also opens new research fields in post-transcriptional regulation of gene expression related to the fine-tuning of cell proliferation, ribosome biogenesis and DNA damage response.

Methods

Plasmids and cloning strategies

Plasmids coding for STAU2^{52}-FLAG$_3$ and STAU2^{59}-FLAG$_3$ were previously described [25]. To generate the retroviral pMSCVpuro-STAU2^{52}-BioID-HA construction, STAU2^{52} was PCR-amplified using Phusion polymerase (NEB) and STAU2^{52}-FLAG$_3$ as template (FW: 5' TAAGCAGCTAGCATGCTTCAAATAAATCAGATGTTCT 3'; RV: 5' TGCTTAACCGGTCTACCTGAAAGCCTTGAATCCT 3'). The PCR product was digested by NheI and AgeI and cloned into pcDNA3.1 BioID2-HA vector [MCS-BioID2-HA was a gift from Kyle Roux (Addgene plasmid # 74224 ; http://n2t.net/addgene:74224; RRID:Addgene_74224)] [74]. The resulting product was PCR-amplified and cloned into retroviral pMSCV puromycin vector after EcoRV digestion (FW: 5' GCTAGCATGCTTCAAATAAAT 3; RV: 5' GTTTAAACTTAAGCTTCTATGCG 3'). Three copies of the myc sequence were introduced at the NotI site.

To generate the retroviral pMSCVpuro-STAU2^{52}-TurboID-HA and pMSCVpuro-YFP-TurboID-HA vectors, STAU2^{52}-FLAG and YFP were PCR-amplified using Phusion polymerase (NEB) and oligonucleotide primers (STAU2: FW: 5' TAAGCAGCGGCCGCATGCTTCAAATAAATCAGATGTTCTCAG 3'; RV: 5'TGCTTAGCTAGCGGATCCGAATTCGAATCCGGAGACGTACGACCGGTCTACCTGAAAGCCTTGAATCCTTG 3') (YFP: FW: 5' TAAGCAGCGGCCGCGCCACCATGGTGAGCAAG 3'; RV: 5' TGCTTAGCTAGCGGATCCGAATTCGAATCCGGAGACGTACGACCGGTCCTTGTACAGCTCGTCCATGC 3'). The PCR products were digested by NotI and NheI and cloned into pcDNA3.1 TurboID-HA vector [V5-TurboID-NES_pCDNA3 was a gift from Alice Ting (Addgene plasmid # 107169; http://n2t.net/addgene:107169; RRID: Addgene_107169)]. The resulting products were PCR-amplified and cloned into retroviral pMSCV puromycin vector after NotI digestion (STAU2: FW: 5' TAAGCAGCGGCCGCGCCACCATGCTTCAAATAAATCAG 3'; RV: 5' TGCTTAGCGGCCGCCTATGCGTAATCCGGTACATCGTAAGGGTATCCCTTTTCGGCAGACCGCAG 3') (YFP:

FW: 5’ TAAGCAGCGGCCGCGCCACCATGGTGAGCAAG 3’; RV: 5’ TGCTTAGCGGCCGCTTACTATGCGTAATCCGGTACATCGTAAGGGTATCCGTCCAGGGTCAGGCGCTC 3’).

Generation of STAU2-KO hTERT-RPE1 cell lines and genomic sequencing

hTERT-RPE1 cells were transfected with a plasmid coding for GFP, Cas9, and a sgRNA targeting exon 6 of the *STAU2* gene (Horizon Discovery). Forty-eight hours post-transfection, GFP positive cells were sorted by FACS and plated into a 10 cm dish. Forty-eight hours after the first sorting, cells were once again isolated by FACS, and individual cells were grown into 96-well plates until colonies formed. The loss of STAU2 expression was monitored by dot blotting using anti-STAU2 antibody. Genomic DNA of several clones was isolated (Genomic DNA Miniprep Kit, Bio Basic) and PCR-amplified with specifics primers flanking exon 6 of the *STAU2* gene (FW: 5’ AGCAGAATTCTTGGATAGGATAGAACAGAATTTGG 3’; RV: 5’ ATTAGGATCCACACACATAGCAGACAACATAAC 3’). PCR products were cloned into a pBluescript SK (+) vector (Stratagene) and sequenced (Sanger Sequencing Services Genome Québec).

Antibodies and reagent

Primary Antibodies against CHK1 (2G1D5), PARP1 (46D11), H2AX (D17A3), and H2AX (20E3) were purchased from Cell Signaling; against GAPDH (0411), HA (12CA5) and Myc (9E10) were purchased from Santa Cruz Biotechnology. Anti-STAU2 (HPA019155), anti-β-Actin (A5441), anti-Flag (F3165), and HRP-Streptavidin were obtained from Sigma. All primary antibodies were used at 1:1000 dilution. MG132 (C2211), iCHK1 (681 637) and DMSO were purchased from Millipore-Sigma; ZVAD-FMK (S7023), Emricasan (S7775), PF47 (PF-477736, S2904), and CHIR124 (S2683) were obtained from Selleckchem.

Cell culture

hTERT-RPE1, HCT116 and HeLa cells were cultured in Dulbecco modified Eagle’s medium (DMEM, Wisent) supplemented with 10% fetal bovine serum (Wisent), 100 µg/ml streptomycin and 100 units/ml penicillin (Wisent) under 5% CO2 atmosphere.

DNA transfection and infection

For transient expression, cells were transfected with lipofectamine 2000 (Invitrogen) or Mirus X2 (Mirus Bio. LLC) at approximatively 60% confluency. For infections, Phoenix cells were transfected at approximatively 50% confluency using lipofectamine 2000, with 10 µg of retroviral plasmids (pMSCV-puromycin) and 5 µg of packaging plasmid. Virus-containing supernatant were collected, filtered (0.45 µm), and added to target cells (HCT116, hTERT-RPE1) with polybrene (8 µg/ml). Infected cells were selected on puromycin (HCT116, 2 µg/ml; hTERT-RPE1, 5 µg/ml).

Protein Electrophoresis and Western blot analysis

Total cell extracts were prepared in lysis buffer (50 mM Tris–HCl pH 7.5, 15 mM EDTA, 0.5% Triton X-100, 100 mM NaCl, 1 mM dithiothreitol [DTT] and a protease inhibitor cocktail [Roche]), resolved by SDS–polyacrylamide gel electrophoresis and transferred to nitrocellulose membrane. Membranes were blocked

in 5% milk at room temperature and incubated with primary antibodies overnight at 4 °C prior to incubation with HRP-conjugated secondary antibody [polyclonal anti-mouse (1/3000), Dako: P0447; polyclonal anti-rabbit (1/5000), Dako: P0448] for 1 hour at room temperature. Membranes were processed using Perkin Elmer Western Lightning Plus-ECL. Data were collected either on X-ray films (Fujifilm) or with the ChemiDoc MP Imaging System (Bio-Rad Laboratories). Western blot signals were quantified with the ImageLab (Bio-Rad Laboratories) software or with ImageJ software (NIH.gov). For the detection of biotinylated proteins by western blot, membranes were blocked in PBS-BSA 5% and incubated with HRP-streptavidin 0.3% in PBS-BSA 3% for 45 min at room temperature.

RNA isolation and RT-qPCR

Total RNA was isolated from cell extracts using the Geneaid extraction kit. Purified RNA was resuspended in 40 µl of water and digested with DNase using the TURBO DNA-free kit (Ambion). Reverse transcription reactions were done with 1 µg of RNA using RevertAid H Minus First Strand cDNA Synthesis kit (Thermo Scientific. qPCR was performed with Luna® Universal qPCR Master Mix (NEB) on a LightCycler 96 instrument (Roche). Samples were run in triplicates and normalized to actin expression.

Cell growth assays

To determine cell proliferation rates, cells were plated at the same density (Growth curve assay: HeLa: 5000 cells, hTERT-RPE1: 8000 cells and HCT116 5000 cells. Colony assay: HeLa 15 000 cells, hTERT-RPE1: 15 000 or 25 000 cells, HCT116 15 000 cells) and allowed to grow for 9 days. Cell proliferation was quantified using a crystal violet retention assay (39). For growth curve assay, cells were harvested every day and the number of cells was counted with an automated hemacytometer.

BioID2 and TurboID sample preparations

One (TurboID) or two (BioID2) biological replicates were processed independently as described [75]. Briefly, stable cell line expressing STAU2^{52}-BioID-HA, STAU2^{52}-TurboID-HA, or YFP-TurboID-HA were generated by retroviral infection. Cells were incubated in the presence of 50 µM biotin for 16 h (BioID2) or 4 h (TurboID) and lysed in 700 µL RIPA lysis buffer (50 mM Tris pH 8, 150 mM NaCl, 0.1% SDS, 0.5% sodium deoxycholate, 1% Triton X-100, 1 × protease inhibitor cocktail, Sigma-Aldrich). Cell extracts were sonicated and biotinylated proteins pulled down with 250 µL streptavidin-coated magnetic beads (Dynabeads MyOne Streptavidin T1). Beads were then washed twice with 1 mL of RIPA lysis buffer, once with 1 mL of 1 M KCl, once with 1 mL of 0.1 M Na2CO3, once with 1 mL of 2 M urea in 10 mM Tris-HCl (pH 8.0), and twice with 1 mL RIPA lysis buffer. Beads were then resuspended in 100 µL 50 mM ammonium bicarbonate solution, and proteins identified at the proteomic core facility for LC-MS/MS analysis.

Protein identification

The peak list files were generated with Proteome Discoverer (version 2.1) using the following parameters: minimum mass set to 500 Da, maximum mass set to 6000 Da, no grouping of MS/MS spectra, precursor charge set to auto, and minimum number of fragment ions set to 5. Protein database searching was

performed with Mascot 2.6 (Matrix Science) against the Uniprot human protein database (May 16th, 2018). The mass tolerances for precursor and fragment ions were set to 10 ppm and 0.6 Da, respectively. Trypsin was used as the enzyme allowing for up to 1 missed cleavage. Cysteine carbamidomethylation was specified as a fixed modification, and methionine oxidation as variable modifications. Data interpretation was performed using Scaffold (version 4.8.9). Protein lists were submitted to the CRAPome software and proteins were sorted by SAINT score, or the fold change scores (FC-A, FC-B). Proteins with SAINT probability (SP) greater than 0.7 were selected. REPRINT tools were used to generate visual analysis of our mass spectrometry data.

Epifluorescence microscopy

Cells were seeded onto 12 × 12 mm glass coverslips in 6-well plates and incubated overnight at 37 °C. Cells were fixed in 4% PFA for 15 minutes at room temperature and permeabilized in 10 mM Tris (pH 7.5), 0.5% Triton-X-100 (v/v) and 0.1% BSA (w/v) for 10 minutes. Cells were then stained with anti-myc (1:600) or anti-HA: (1:500) for 1 h at room temperature. Secondary antibody (Alexa Fluor 488 goat) was added for 1 h at room temperature. Coverslips were washed once with PBS and incubated for 10 min with PBS containing DAPI (0.5 µg/ml) at room temperature. Coverslips were mounted using Dako mounting medium (Dako Faramount Aqueous Mounting Medium; S3025). Images were acquired with an ECLIPSE TE2000U microscope (NIKON). Images processing was performed using Metamorph (Molecular Devices) or ImageJ software. The data are representative of at least 15 fields of view.

List Of Abreviations

STAU2, Staufen2. CRISPR, Clustered Regularly Interspaced Short Palindromic Repeats. CHK1, checkpoint kinase 1. DDR, DNA damage response. RBP, RNA-binding protein. KO, knockout. WT, wild type. shRNA, short hairpin RNA. GO, gene ontology. lncRNA, long non-coding RNA. CRAPome, Contaminant Repository for Affinity Purification. REPRINT, Resource for Evaluation of Protein Interaction Networks. SAINT, Significance Analysis of INTeractome.

Declarations

Ethics approval and consent to participate

Not applicable.

Consent for publication

Not applicable.

Availability of data and materials

All data generated or analysed during this study are included in this published article [and its supplementary information files].

Competing interests

The authors declare that they have no competing interests

Funding

This work was supported by a grant (RGPIN-2019-05027) from the Natural Sciences and Engineering Research Council of Canada (NSERC) to LDG. The funding agency had no role in the design of the study and collection, analysis, and interpretation of data and in writing the manuscript.

Authors' contributions

LC and RB acquired data. LC, RB and LDG designed the work, analyzed and interpreted data. LC and LDG wrote the manuscript. LC, RB and LDG approved the final version, including author’s contributions to the study.

Acknowledgements

We thank Dr. Xin Zhang for useful suggestions, Louise Cournoyer for help with cell culture, Alicia Pellerin-Viger, Bellastrid Doran, Yulemi Gonzalez Quesada for technical assistance, and Dr. Armelle Le Campion for her support with flow cytometry. We also thank the proteomic core facilities at the Institut de Recherches en Immunologie et Cancer (IRIC) for the proteomics analysis.

References

1. Hong S. RNA Binding Protein as an Emerging Therapeutic Target for Cancer Prevention and Treatment. J Cancer Prev. 2017;22(4):203–10.
2. Moore S, Jarvelin AI, Davis I, Bond GL, Castello A. Expanding horizons: new roles for non-canonical RNA-binding proteins in cancer. Curr Opin Genet Dev. 2017;48:112–20.
3. Pereira B, Billaud M, Almeida R. RNA-Binding Proteins in Cancer: Old Players and New Actors. Trends Cancer. 2017;3(7):506–28.
4. Keene JD. RNA regulons: coordination of post-transcriptional events. Nature reviews. 2007;8(7):533–43.
5. Huang R, Han M, Meng L, Chen X. Transcriptome-wide discovery of coding and noncoding RNA-binding proteins. Proc Natl Acad Sci USA. 2018;115(17):E3879-E87.
6. Lukong KE, Chang KW, Khandjian EW, Richard S. RNA-binding proteins in human genetic disease. Trends Genet. 2008;24(8):416–25.
7. Castello A, Fischer B, Hentze MW, Preiss T. RNA-binding proteins in Mendelian disease. Trends Genet. 2013;29(5):318–27.
8. Buchner G, Bassi MT, Andolfi G, Ballabio A, Franco B. Identification of a novel homolog of the Drosophila staufen protein in the chromosome 8q13-q21.1 region. Genomics. 1999;62(1):113–8.

9. Duchaine TF, Hemraj I, Furic L, Deitinghoff A, Kiebler MA, DesGroseillers L. Staufen2 isoforms localize to the somatodendritic domain of neurons and interact with different organelles. Journal of cell science. 2002;115(Pt 16):3285–95.
10. Furic L, Maher-Laporte M, DesGroseillers L. A genome-wide approach identifies distinct but overlapping subsets of cellular mRNAs associated with Staufen1- and Staufen2-containing ribonucleoprotein complexes. RNA (New York, NY. 2008;14(2):324 – 35.
11. Macchi P, Brownawell AM, Grunewald B, DesGroseillers L, Macara IG, Kiebler MA. The brain-specific double-stranded RNA-binding protein Staufen2: nucleolar accumulation and isoform-specific exportin-5-dependent export. J Biol Chem. 2004;279(30):31440–4.
12. Tang SJ, Meulemans D, Vazquez L, Colaco N, Schuman E. A role for a rat homolog of staufen in the transport of RNA to neuronal dendrites. Neuron. 2001;32(3):463–75.
13. Goetze B, Tuebing F, Xie Y, Dorostkar MM, Thomas S, Pehl U, et al. The brain-specific double-stranded RNA-binding protein Staufen2 is required for dendritic spine morphogenesis. J Cell Biol. 2006;172(2):221–31.
14. O'Leary DA, Sharif O, Anderson P, Tu B, Welch G, Zhou Y, et al. Identification of small molecule and genetic modulators of AON-induced dystrophin exon skipping by high-throughput screening. PLoS ONE. 2009;4(12):e8348.
15. Lebeau G, Miller LC, Tartas M, McAdam R, Laplante I, Badeaux F, et al. Staufen 2 regulates mGluR long-term depression and Map1b mRNA distribution in hippocampal neurons. Learning & memory (Cold Spring Harbor, NY. 2011;18(5):pp. 314–26.
16. Park E, Gleghorn ML, Maquat LE. Staufen2 functions in Staufen1-mediated mRNA decay by binding to itself and its paralog and promoting UPF1 helicase but not ATPase activity. Proc Natl Acad Sci USA. 2013;110(2):405–12.
17. Ramasamy S, Wang H, Quach HN, Sampath K. Zebrafish Staufen1 and Staufen2 are required for the survival and migration of primordial germ cells. Developmental biology. 2006;292(2):393–406.
18. Bilogan CK, Horb ME. Xenopus staufen2 is required for anterior endodermal organ formation. Genesis. 2012;50(3):251–9.
19. Cao Y, Du J, Chen D, Wang Q, Zhang N, Liu X, et al. RNA- binding protein Stau2 is important for spindle integrity and meiosis progression in mouse oocytes. Cell cycle (Georgetown Tex. 2016;15(19):2608–18.
20. Cockburn DM, Charish J, Tassew NG, Eubanks J, Bremner R, Macchi P, et al. The double-stranded RNA-binding protein Staufen 2 regulates eye size. Mol Cell Neurosci. 2012;51(3–4):101–11.
21. Kusek G, Campbell M, Doyle F, Tenenbaum SA, Kiebler M, Temple S. Asymmetric Segregation of the Double-Stranded RNA Binding Protein Staufen2 during Mammalian Neural Stem Cell Divisions Promotes Lineage Progression. Cell Stem Cell. 2012;11(4):505–16.
22. Vessey JP, Amadei G, Burns SE, Kiebler MA, Kaplan DR, Miller FD. An Asymmetrically Localized Staufen2-Dependent RNA Complex Regulates Maintenance of Mammalian Neural Stem Cells. Cell Stem Cell. 2012;11(4):517–28.

23. Berger SM, Fernandez-Lamo I, Schonig K, Moya SMF, Ehses J, Schieweck R, et al. Forebrain-specific, conditional silencing of Staufen2 alters synaptic plasticity, learning, and memory in rats. Genome biology. 2017;18.
24. Popper B, Demleitner A, Bolivar VJ, Kusek G, Snyder-Keller A, Schieweck R, et al. Staufen2 deficiency leads to impaired response to novelty in mice. Neurobiol Learn Mem. 2018;150:107–15.
25. Zhang X, Trepanier V, Beaujois R, Viranaicken W, Drobetsky E, DesGroseillers L. The downregulation of the RNA-binding protein Staufen2 in response to DNA damage promotes apoptosis. Nucleic acids research. 2016;44(8):3695–712.
26. McArthur K, Kile BT. Apoptotic Caspases: Multiple or Mistaken Identities? Trends in cell biology. 2018;28(6):475–93.
27. Choi H, Larsen B, Lin ZY, Breitkreutz A, Mellacheruvu D, Fermin D, et al. SAINT: probabilistic scoring of affinity purification-mass spectrometry data. Nature methods. 2011;8(1):70–3.
28. Mellacheruvu D, Wright Z, Couzens AL, Lambert JP, St-Denis NA, Li T, et al. The CRAPome: a contaminant repository for affinity purification-mass spectrometry data. Nature methods. 2013;10(8):730-+.
29. Elbarbary RA, Li W, Tian B, Maquat LE. STAU1 binding 3' UTR IRAlus complements nuclear retention to protect cells from PKR-mediated translational shutdown. Genes Dev. 2013;27(13):1495–510.
30. Beaujois R, Ottoni E, Zhang X, Gagnon C, HSine S, Mollet S, et al. The M-phase specific hyperphosphorylation of Staufen2 involved the cyclin-dependent kinase CDK1. Bmc Cell Biol. 2017;18.
31. Lessard F, Igelmann S, Trahan C, Huot G, Saint-Germain E, Mignacca L, et al. Senescence-associated ribosome biogenesis defects contributes to cell cycle arrest through the Rb pathway. Nat Cell Biol. 2018;20(7):789–99.
32. Elvira G, Massie B, DesGroseillers L. The zinc-finger protein ZFR is critical for Staufen 2 isoform specific nucleocytoplasmic shuttling in neurons. Journal of neurochemistry. 2006;96(1):105–17.
33. Maher-Laporte M, Berthiaume F, Moreau M, Julien LA, Lapointe G, Mourez M, et al. Molecular composition of staufen2-containing ribonucleoproteins in embryonic rat brain. PLoS ONE. 2010;5(6):e11350.
34. Gottlieb TM, Jackson SP. The DNA-dependent protein kinase: requirement for DNA ends and association with Ku antigen. Cell. 1993;72(1):131–42.
35. Morchikh M, Cribier A, Raffel R, Amraoui S, Cau J, Severac D, et al. HEXIM1 and NEAT1 Long Non-coding RNA Form a Multi-subunit Complex that Regulates DNA-Mediated Innate Immune Response. Molecular cell. 2017;67(3):387–99. e5.
36. Jonsson M, Lundwall A, Malm J. The semenogelins: proteins with functions beyond reproduction? Cell Mol Life Sci. 2006;63(24):2886–8.
37. Huttlin EL, Ting L, Bruckner RJ, Gebreab F, Gygi MP, Szpyt J, et al. The BioPlex Network: A Systematic Exploration of the Human Interactome. Cell. 2015;162(2):425–40.

38. Parapuram SK, Chang B, Li L, Hartung RA, Chalam KV, Nair-Menon JU, et al. Differential effects of TGFbeta and vitreous on the transformation of retinal pigment epithelial cells. Invest Ophthalmol Vis Sci. 2009;50(12):5965–74.
39. Sommer G, Dittmann J, Kuehnert J, Reumann K, Schwartz PE, Will H, et al. The RNA-binding protein La contributes to cell proliferation and CCND1 expression. Oncogene. 2011;30(4):434–44.
40. Cookson MR. RNA-binding proteins implicated in neurodegenerative diseases. Wiley Interdiscip Rev RNA. 2017;8(1).
41. Shortt J, Johnstone RW. Oncogenes in cell survival and cell death. Cold Spring Harb Perspect Biol. 2012;4(12).
42. Hills SA, Diffley JF. DNA replication and oncogene-induced replicative stress. Curr Biol. 2014;24(10):R435-44.
43. Ahmed D, Eide PW, Eilertsen IA, Danielsen SA, Eknaes M, Hektoen M, et al. Epigenetic and genetic features of 24 colon cancer cell lines. Oncogenesis. 2013;2:e71.
44. Mittelman D, Wilson JH. The fractured genome of HeLa cells. Genome biology. 2013;14(4):111.
45. Myers K, Gagou ME, Zuazua-Villar P, Rodriguez R, Meuth M. ATR and Chk1 suppress a caspase-3-dependent apoptotic response following DNA replication stress. PLoS Genet. 2009;5(1):e1000324.
46. Zhao H, Piwnica-Worms H. ATR-mediated checkpoint pathways regulate phosphorylation and activation of human Chk1. Molecular cellular biology. 2001;21(13):4129–39.
47. Jackson SP, Bartek J. The DNA-damage response in human biology and disease. Nature. 2009;461(7267):1071–8.
48. Blasius M, Forment JV, Thakkar N, Wagner SA, Choudhary C, Jackson SP. A phospho-proteomic screen identifies substrates of the checkpoint kinase Chk1. Genome biology. 2011;12(8):R78.
49. McIlwain DR, Berger T, Mak TW. Caspase functions in cell death and disease. Cold Spring Harb Perspect Biol. 2013;5(4):a008656.
50. Patil M, Pabla N, Dong Z. Checkpoint kinase 1 in DNA damage response and cell cycle regulation. Cell Mol Life Sci. 2013;70(21):4009–21.
51. Li J, Yuan J. Caspases in apoptosis and beyond. Oncogene. 2008;27(48):6194–206.
52. Kuranaga E. Beyond apoptosis: caspase regulatory mechanisms and functions in vivo. Genes Cells. 2012;17(2):83–97.
53. Baena-Lopez LA, Arthurton L, Xu DC, Galasso A. Non-apoptotic Caspase regulation of stem cell properties. Semin Cell Dev Biol. 2018;82:118–26.
54. Petermann E, Woodcock M, Helleday T. Chk1 promotes replication fork progression by controlling replication initiation. Proc Natl Acad Sci USA. 2010;107(37):16090–5.
55. Wilsker D, Petermann E, Helleday T, Bunz F. Essential function of Chk1 can be uncoupled from DNA damage checkpoint and replication control. Proc Natl Acad Sci USA. 2008;105(52):20752–7.
56. Rodriguez R, Meuth M. Chk1 and p21 cooperate to prevent apoptosis during DNA replication fork stress. Molecular biology of the cell. 2006;17(1):402–12.

57. Meuth M. Chk1 suppressed cell death. Cell division. 2010;5:21.
58. Kim HH, Abdelmohsen K, Gorospe M. Regulation of HuR by DNA Damage Response Kinases. Journal of nucleic acids. 2010;2010.
59. Thomas MG, Martinez Tosar LJ, Loschi M, Pasquini JM, Correale J, Kindler S, et al. Staufen recruitment into stress granules does not affect early mRNA transport in oligodendrocytes. Molecular biology of the cell. 2005;16(1):405–20.
60. Lindstrom MS, Jurada D, Bursac S, Orsolic I, Bartek J, Volarevic S. Nucleolus as an emerging hub in maintenance of genome stability and cancer pathogenesis. Oncogene. 2018;37(18):2351–66.
61. Kiebler MA, Jansen RP, Dahm R, Macchi P. A putative nuclear function for mammalian Staufen. Trends Biochem Sci. 2005;30(5):228–31.
62. Takeuchi Y, Horiuchi T, Kobayashi T. Transcription-dependent recombination and the role of fork collision in yeast rDNA. Genes Dev. 2003;17(12):1497–506.
63. Garcia-Muse T, Aguilera A. Transcription-replication conflicts: how they occur and how they are resolved. Nat Rev Mol Cell Biol. 2016;17(9):553–63.
64. Zou L, Elledge SJ. Sensing DNA damage through ATRIP recognition of RPA-ssDNA complexes. Science (New York. 2003;300(5625):pp. 1542–8.
65. Shechter D, Costanzo V, Gautier J. ATR and ATM regulate the timing of DNA replication origin firing. Nat Cell Biol. 2004;6(7):648–55.
66. Jazayeri A, Falck J, Lukas C, Bartek J, Smith GC, Lukas J, et al. ATM- and cell cycle-dependent regulation of ATR in response to DNA double-strand breaks. Nat Cell Biol. 2006;8(1):37–45.
67. Li X, Manley JL. Cotranscriptional processes and their influence on genome stability. Genes Dev. 2006;20(14):1838–47.
68. Aguilera A, Gomez-Gonzalez B. Genome instability: a mechanistic view of its causes and consequences. Nature reviews. 2008;9(3):204–17.
69. Hamperl S, Cimprich KA. The contribution of co-transcriptional RNA:DNA hybrid structures to DNA damage and genome instability. DNA Repair. 2014;19:84–94.
70. Paulsen RD, Soni DV, Wollman R, Hahn AT, Yee MC, Guan A, et al. A genome-wide siRNA screen reveals diverse cellular processes and pathways that mediate genome stability. Molecular cell. 2009;35(2):228–39.
71. Su M, Wang H, Wang W, Wang Y, Ouyang L, Pan C, et al. LncRNAs in DNA damage response and repair in cancer cells. Acta Biochim Biophys Sin (Shanghai). 2018;50(5):433–9.
72. Lees-Miller SP, Beattie TL, Tainer JA. Noncoding RNA joins Ku and DNA-PKcs for DNA-break resistance in breast cancer. Nat Struct Mol Biol. 2016;23(6):509–10.
73. Dianatpour A, Ghafouri-Fard S. The Role of Long Non Coding RNAs in the Repair of DNA Double Strand Breaks. Int J Mol Cell Med. 2017;6(1):1–12.
74. Kim DI, Jensen SC, Noble KA, Kc B, Roux KH, Motamedchaboki K, et al. An improved smaller biotin ligase for BioID proximity labeling. Molecular biology of the cell. 2016;27(8):1188–96.

75. Branon TC, Bosch JA, Sanchez AD, Udeshi ND, Svinkina T, Carr SA, et al. Efficient proximity labeling in living cells and organisms with TurboID. Nat Biotechnol. 2018;36(9):880-+.
76. Tripathi S, Pohl MO, Zhou YY, Rodriguez-Frandsen A, Wang GJ, Stein DA, et al. Meta- and Orthogonal Integration of Influenza "OMICs" Data Defines a Role for UBR4 in Virus Budding. Cell Host Microbe. 2015;18(6):723–35.

Figures

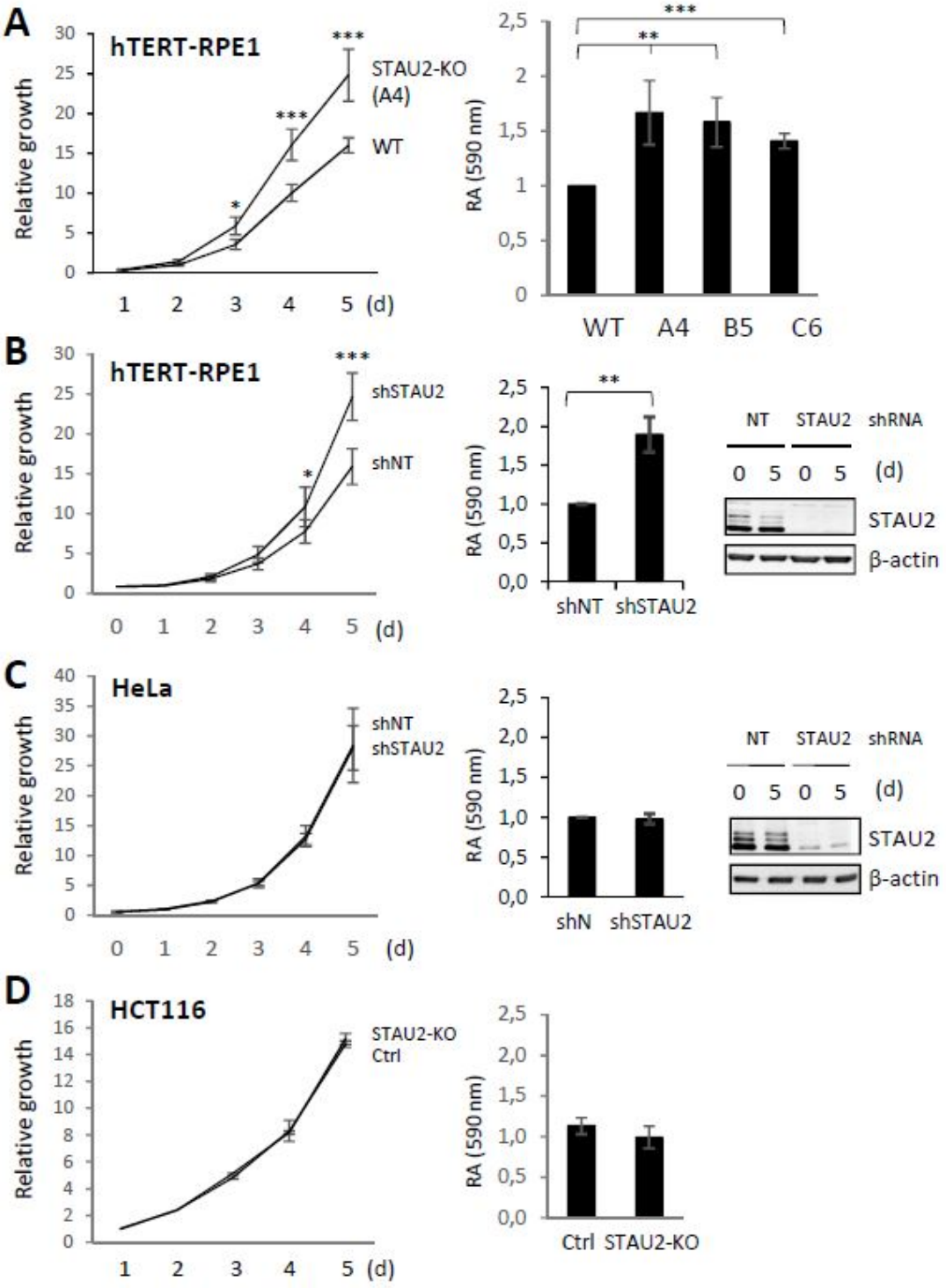

Figure 1

STAU2 depletion facilitates cell proliferation in hTERT-RPE1 cells. Growth curves (left panels) and colony growth assays (right panels) were used to monitor cell proliferation. All the graphs show the means and standard deviation of at least three independently performed experiments. The relative growth of wild-type cells was arbitrary fixed to 1 for the colony assays. *** p-value ≤ 0.001; ** p-value ≤ 0.01; * p-value ≤ 0.05. Two-tailed Student's t-test for growth curves analysis. One sample t-test for the colony assay. (A)

STAU2-KO clones (A4, B5, C6) and wild-type (WT) hTERT-RPE1 cells. n=4. (B) hTERT-RPE1 cells were infected with viruses expressing shRNA control (shNT) or shRNA against STAU2 (shSTAU2). n=4. (C) HeLa cells were infected with viruses expressing shRNA control (shNT) or shRNA against STAU2 (shSTAU2). n=4. (D) CRISPR-mediated STAU2-KO HCT116 (STAU2-KO) and CRISPR-treated cells that still express STAU2 as controls (Ctrl). n=3. (B,C) Representative Western blots showing STAU2 expression.

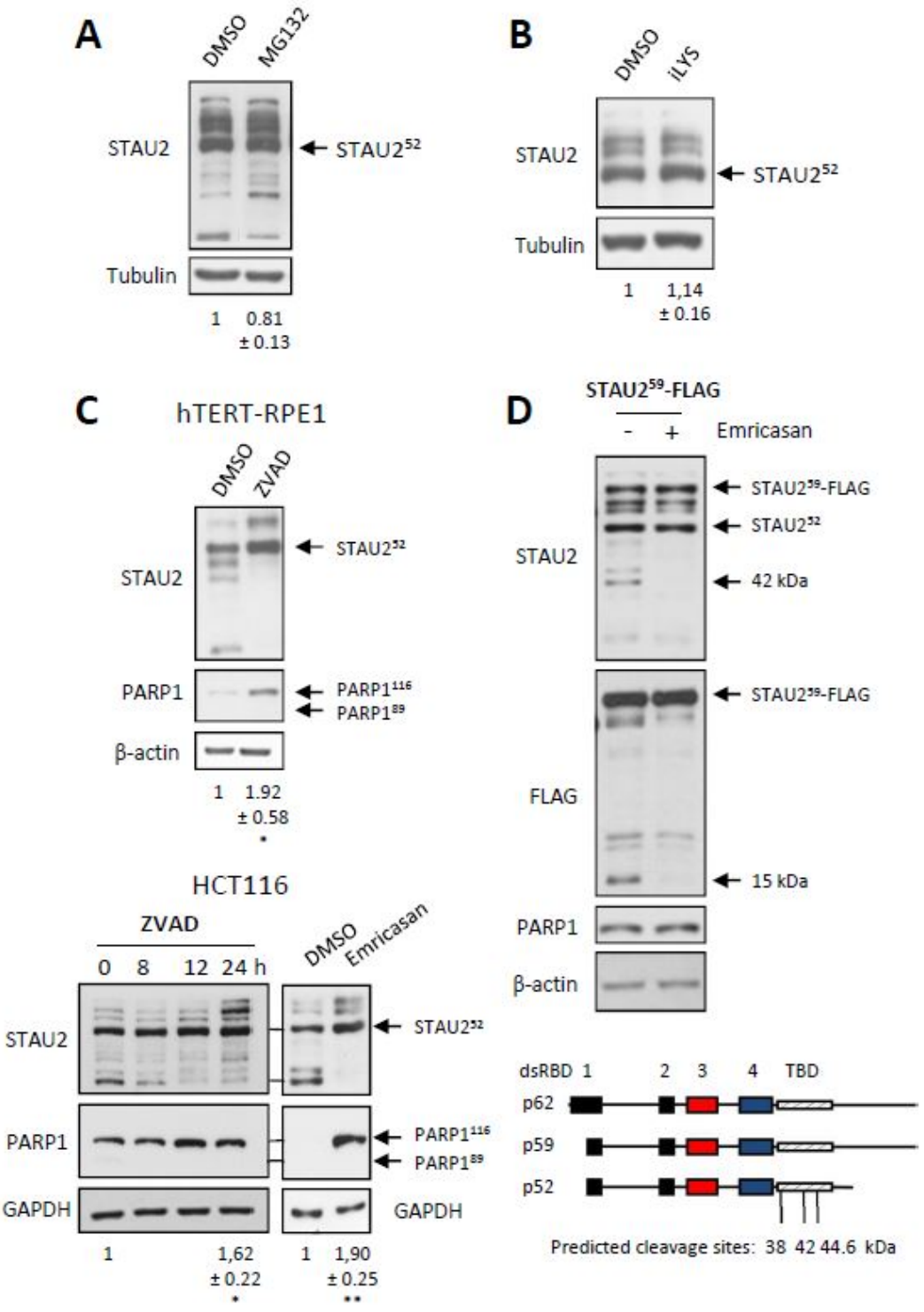

Figure 2

STAU2 is a target of caspase(s). Cells were incubated in the presence of different peptidase inhibitors as indicated or DMSO (vehicle). Cell extracts were analyzed by Western blotting for STAU2 expression. All Western blots are representative of three independently performed experiments that gave similar results. Quantification of STAU2 protein levels is indicated below the gels. The ratio of STAU2 on the loading control in DMSO-treated cells was fixed to 1. * p-value ≤ 0.05; ** p-value ≤ 0.01. One sample t-test. PARP1 was used as a measure of caspase inhibition. (A, B) HCT116 cells were incubated in the presence of the proteasome inhibitor MG132 (10 μM) for 6 h (A) or the lysosome inhibitor iLYS (10 μM) for 10 h (B). (C) hTERT-RPE1 (top) and HCT116 (bottom) cells were incubated in the presence of caspase inhibitors: ZVAD-FMK (50 μM for 8 h) and/or emricasan (40 μM for 24 h). (D) HCT116 cells were transfected with a plasmid coding for STAU259-FLAG3. Cells were then incubated in the presence of DMSO (-) or of the caspase inhibitor Emricasan (40 μM) (+) for 24 h. Full length and degradation fragments were visualized by anti-STAU2 and anti-FLAG antibodies to detect the N- and C-terminal ends of STAU2, respectively. Western blots are representative of two independently performed experiments. β-actin was used as a loading control. (bottom) Schematic representation of STAU2 protein. Predicted caspase cleavage sites are shown. Red and blue boxes: major and minor RNA-binding domains, respectively. Black boxes, regions with RNA-binding consensus sequence but lacking RNA-binding activity in vitro. Hatched boxes, tubulin-binding domain.

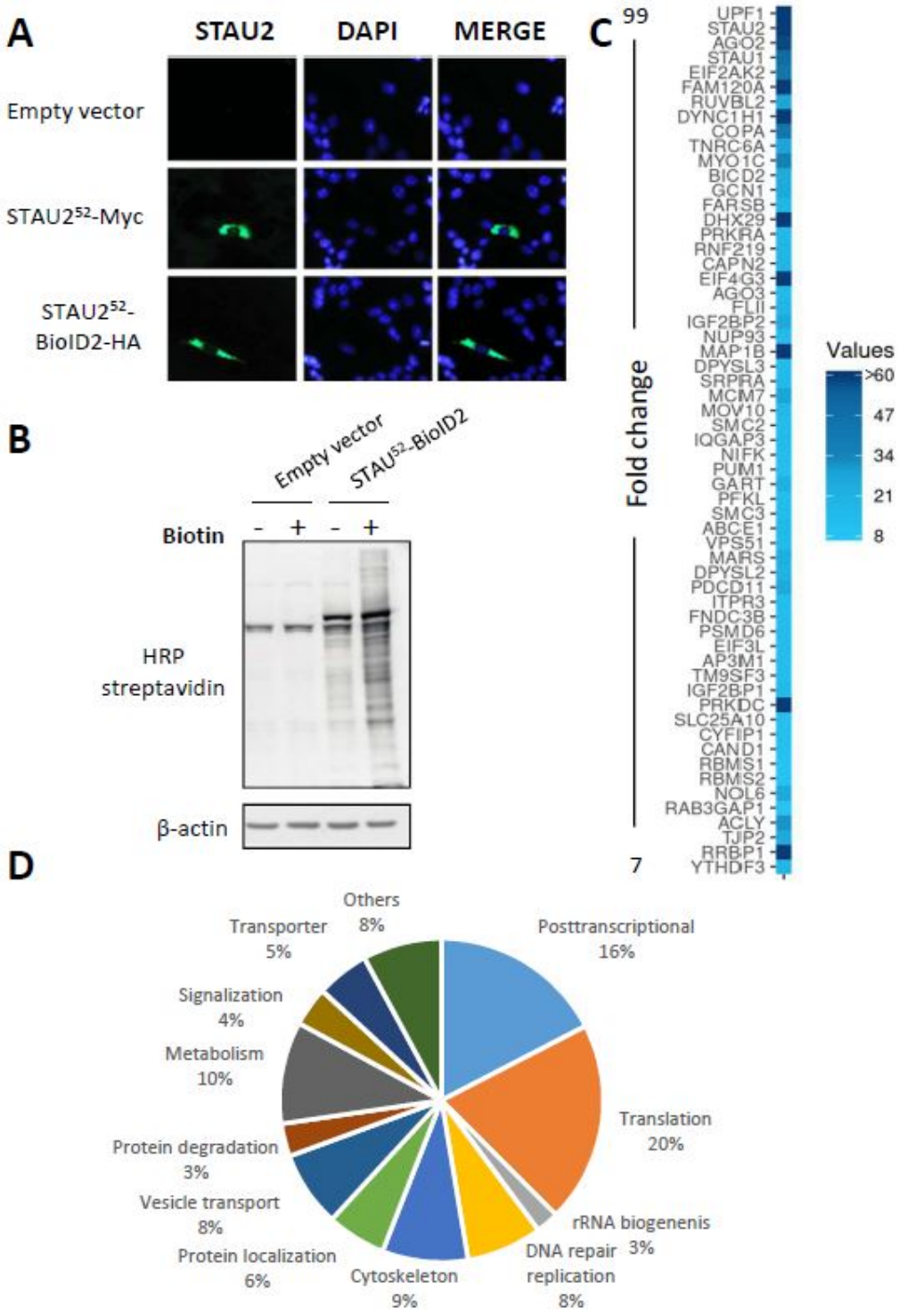

Figure 3

Identification of proteins in proximity to STAU2. (A) Control (empty vector), STAU252-myc3 and STAU252-BioID2-HA infected cells were analyzed by immunofluorescence using anti-Myc and anti-HA antibodies to compare the subcellular localization of STAU2-tagged proteins. DAPI was used to stain the nucleus. (B) hTERT-RPE1 cells were infected with viruses expressing an empty vector or STAU252-BioID2-HA. Two days post selection, cells were incubated in the absence (-) or presence (+) of 50 µM biotin for 16 hours.

Biotinylated proteins were visualized by Western blotting using streptavidin-coupled HRP. (C) 60 proteins with the best interaction probability scores are listed along with a heat map representing the average spectral counts of STAU2 interactors. (D) Pie chart of the percentage of STAU2 interactors associated with different biological processes.

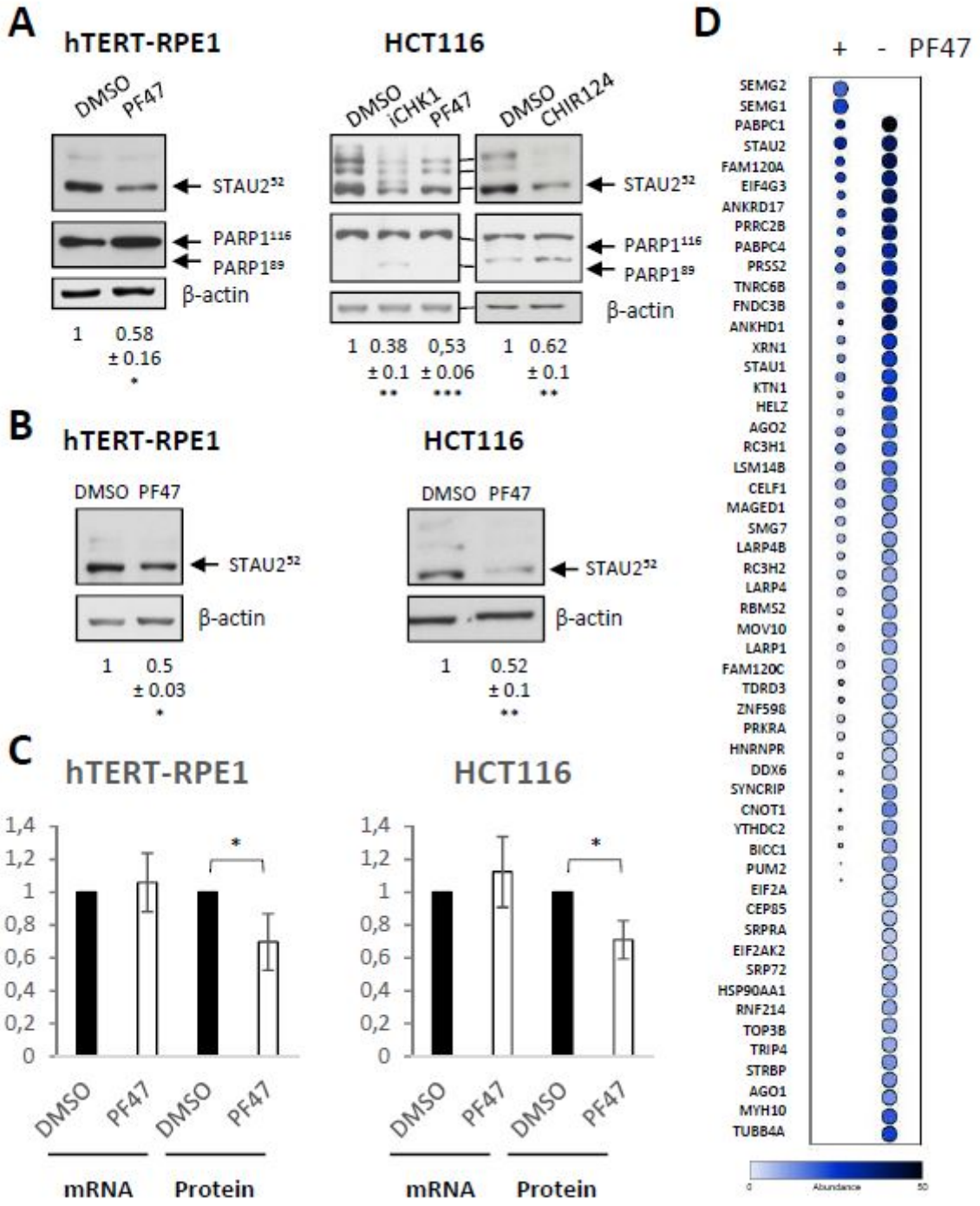

Figure 4

CHK1 inhibition causes a decrease in the steady-state levels of STAU2 protein. hTERT-RPE1 (left) and/or HCT116 (right) cells were incubated in the presence of CHK1 inhibitors. Cell extracts were analyzed by Western blotting. The vehicle DMSO was used as control and β-actin as a loading control. PARP1 cleavage was used as a measure of apoptosis. Quantification of STAU2 protein levels is indicated below the blots. Western blots are representative of three independently performed experiments that gave similar results. (A) Cells were incubated in the presence of CHK1 inhibitors (PF47 20 μM, iCHK1 20 μM for 8.5 h and CHIR124 200 nM for 24 h). (B) Cells were incubated in the presence of low concentration of the CHK1 inhibitor PF47 (1 μM) for 48 h. (C) Cells were incubated in the presence of CHK1 inhibitors (PF47 20 μM) for 6.5 h. STAU2 protein expression was analyzed by western blotting, while STAU2 mRNA levels were quantified by RT-qPCR. The ratio of STAU2 (protein or mRNA) on actin (protein or mRNA, respectively) in DMSO-treated cells was fixed to 1. Protein and mRNA quantification represents the means and standard deviation of three independently performed experiments. * p-value ≤ 0.05. ** p-value ≤ 0.01; *** p-value ≤0.001. One sample t-test. (D) Dotplot representation of protein abundance in proximity to STAU2 in the presence or absence of the CHK1 inhibitor PF47. Color range indicates peptide abundance and the size of circles their relative abundance.

Supplementary Files

This is a list of supplementary files associated with this preprint. Click to download.

- SuppTableS8.xlsx
- SuppTableS7.xlsx
- SuppTableS6.xlsx
- SuppTableS5.xlsx
- SuppTableS4.xlsx
- SuppTableS3.xlsx
- SuppTableS2.xlsx
- SuppTableS1.xlsx
- SuppFigS5.pdf
- FigS4.JPG
- FigS3.JPG
- FigS2.JPG
- FigS1.JPG